

---

# Analysis of Softmax Approximation for Deep Classifiers under Input-Dependent Label Noise

---

**Mark Collier**

Google AI

markcollier@google.com

**Basil Mustafa**

Google AI

basilm@google.com

**Efi Kokiopoulou**

Google AI

efi@google.com

**Jesse Berent**

Google AI

jberent@google.com

## Abstract

Modelling uncertainty arising from input-dependent label noise is an increasingly important problem. A state-of-the-art approach for classification places a normal distribution over the softmax logits, where the mean and variance of this distribution are learned deep functions of the inputs [19]. This approach has impressive empirical performance but lacks theoretical justification. We argue that the softmax should be viewed as a smooth approximation (controlled by a temperature parameter) to an argmax in the true data generation process. Under this view, we establish a general framework for modeling input-dependent label noise with deep classifiers, whereby the state-of-the-art method [19] becomes a special case corresponding to the temperature being set to 1.0. We illustrate that the softmax temperature controls a bias-variance trade-off for the approximation and the optimal point on this trade-off is not always found at 1.0. By tuning the softmax temperature, we improve performance on image classification benchmarks with controlled label noise. For image segmentation, where input-dependent label noise naturally arises, tuning the temperature increases the mean IoU on the PASCAL VOC and Cityscapes datasets by more than 1% over the state-of-the-art model.

## 1 Introduction

With deep classification models being deployed in safety critical applications, estimating a model’s uncertainty in its predictive distribution has become a pressing problem [10]. The uncertainty of a classification model can be divided into aleatoric and epistemic uncertainty [19]:

- **Aleatoric uncertainty** captures noise in the dataset’s labels. This uncertainty could be the result of noisy measurements, mis-labelled samples, unobserved predictive variables, and so on. Aleatoric uncertainty can be characterized as homoscedastic or heteroscedastic:
  - **Homoscedastic**: the uncertainty in the labels is constant across the input space.
  - **Heteroscedastic**: the aleatoric uncertainty varies across the input space, e.g. certain examples may be more difficult to label manually than others.
- **Epistemic uncertainty** captures uncertainty about the model that generated the data. This includes but is not limited to uncertainty over the parameters of the model.

The predictive uncertainty of a model is the combination of its aleatoric and epistemic uncertainty. In this paper we address the modelling of aleatoric uncertainty for classification tasks. Our approach can be easily combined with many approaches in the suite of Bayesian neural networks that estimate the epistemic uncertainty of a model [4, 11, 12] resulting in an estimate of the full predictive uncertainty. However, this is not the focus of this work. We note that epistemic uncertainty reduces to zero in the limit of infinite data, while aleatoric uncertainty is irreducible, so as datasets continue to increase in size, modeling aleatoric uncertainty will increasingly become more important.

If a dataset contains heteroscedastic (i.e., input-dependent) label noise, then modelling heteroscedasticity is crucial for accurate uncertainty quantification and parameter estimation. Maximum likelihood estimation of a non-linear homoscedastic model on heteroscedastic data is biased and inconsistent [13]. Thus, for datasets with such uncertainty, improved heteroscedastic modelling promises improved predictive performance with better calibrated uncertainty. The current best method for deep classifiers trained under heteroscedastic label noise, introduced by Kendall and Gal [19], places a normal distribution over the softmax logits and parameterizes the mean and variance of the normal with deep neural networks. However it is unclear what the corresponding data generation process is to this method.

The main contributions of this paper are:

1. Provide a theoretical framework for deep heteroscedastic classification by viewing the use of the softmax as a smooth approximation to an argmax in the true data generation process. The state-of-the-art method [19] becomes a special case of our framework.
2. Via this framework, establish the importance of the softmax temperature in controlling a bias-variance trade-off for the approximation.
3. Improve image classification and segmentation performance by tuning the softmax temperature. We compare to Kendall and Gal [19] and baselines from the noisy labels literature.

## 2 Background

In order to motivate our development of heteroscedastic classification models we first review a heteroscedastic regression model by Kendall and Gal [19] as it is particularly amenable to interpretation.

### 2.1 Heteroscedastic Regression Models

We have a dataset of examples:  $\{(\mathbf{x}_1, y_1), \dots, (\mathbf{x}_N, y_N)\}$  where  $y_i$  is real valued. We assume that  $y_i$  are i.i.d. such that  $y_i \sim \mathcal{N}(f^{\mathbf{w}}(\mathbf{x}_i), \sigma^{\mathbf{w}}(\mathbf{x}_i)^2)$ , where  $f^{\mathbf{w}}(\mathbf{x}_i)$  and  $\sigma^{\mathbf{w}}(\mathbf{x}_i)$  are parametric models parameterized by  $\mathbf{w}$ . The log-likelihood of the data is:

$$\frac{1}{N} \sum_{i=1}^N \frac{1}{2\sigma^{\mathbf{w}}(\mathbf{x}_i)^2} (y_i - f^{\mathbf{w}}(\mathbf{x}_i))^2 + \frac{1}{2} \log \sigma^{\mathbf{w}}(\mathbf{x}_i)^2. \quad (1)$$

If we set  $\sigma^{\mathbf{w}}(\mathbf{x}_i) = 1$  this reduces to a standard homoscedastic regression model. However for a non-constant function  $\sigma^{\mathbf{w}}(\mathbf{x}_i)$ , this differs from a standard regression model in that the squared error loss for each example is weighted by  $1/2\sigma^{\mathbf{w}}(\mathbf{x}_i)^2$ . Those examples with higher predicted aleatoric uncertainty will be down-weighted in the learning objective, reducing overfitting to noisy labels.

### 2.2 Heteroscedastic Classification Models

Following the development of the heteroscedastic regression model mentioned above, Kendall and Gal [19] develop a similarly structured heteroscedastic classification model, which is the state-of-the-art approach for deep heteroscedastic classification. The method places a Gaussian distribution on the logits of a standard softmax classification model, making the logits latent variables:

$$\begin{aligned} y_c^* &\sim \mathcal{N}(f_c^{\mathbf{w}}(\mathbf{x}), \sigma_c^{\mathbf{w}}(\mathbf{x})^2), \quad \forall c = 1 \dots K, \\ p_c &= \frac{\exp(y_c^*)}{\sum_{k=1}^K \exp(y_k^*)}, \end{aligned} \quad (2)$$

where  $p_c$  is the probability the label is class  $c$  and  $K$  is the number of classes. The model's log-likelihood and a Monte Carlo (MC) method for estimating it are also developed [19].

### 2.3 Latent Variable Classification Models

One way to motivate many standard classification models is to introduce a latent variable into the data generation process. Suppose there is some utility  $y_c^*$  associated with each class. This utility is the sum of a reference utility  $f_c^{\mathbf{w}}(\mathbf{x})$ , which is the function of observed variables and an unobserved

stochastic component  $\epsilon_c$ . Hence  $y_c^*$  is latent and stochastic. Class  $c$  is chosen if its associated utility is greater than the utility for all other classes i.e.  $y = c \Leftrightarrow y_c^* > y_k^*, \forall k \neq c$ . We adopt our terminology from discrete choice models in econometrics where this latent variable formulation is standard [32]. The probability that class  $c$  is chosen is  $p_c = P(\arg \max_k y_k^* = c)$ :

$$\begin{aligned} y_c^* &= f_c^{\mathbf{w}}(\mathbf{x}) + \epsilon_c \\ p_c &= P(y_c^* > y_k^*, \forall k \neq c) = P(\arg \max_k y_k^* = c). \end{aligned} \quad (3)$$

If we assume  $\epsilon_c$  is i.i.d.  $\sim Gumbel(0, 1)$  then  $p_c = \frac{\exp(y_c^*)}{\sum_{k=1}^K \exp(y_k^*)}$  i.e. this latent variable formulation leads to a *multinomial logistic* model which is exactly the softmax classification model with cross-entropy loss widely used with neural networks [32]. Similarly if we choose  $\epsilon_c$  i.i.d.  $\sim \mathcal{N}(0, 1)$  this leads to a *multinomial probit* model with identity covariance matrix [32].

Heteroscedastic models however break the assumption that the additive noise terms are identically distributed. As a result, computing  $p_c$  or its gradient involves an integral over  $\epsilon$  for which no analytic solutions exist [2, 32]. As there is no known closed form solution for  $p_c$  or its gradient we will have to resort to approximation schemes to learn the parameters of our model.

In light of this formulation of heteroscedastic classification models we can revisit the model introduced in Eq. (2), and attempt to cast it similarly as a latent variable model:

$$y_c^* \sim \mathcal{N}(f_c^{\mathbf{w}}(\mathbf{x}), \sigma_c^{\mathbf{w}}(\mathbf{x})^2) \Leftrightarrow y_c^* = f_c^{\mathbf{w}}(\mathbf{x}) + \epsilon_c, \quad \epsilon_c \sim \mathcal{N}(0, \sigma_c^{\mathbf{w}}(\mathbf{x})^2). \quad (4)$$

But if we continue to assume that  $p_c$  is the probability of the latent  $y_c^*$  being maximum, then in general we do not get the same  $p_c$  as assumed by Kendall and Gal [19]:

$$p_c = P(\arg \max_k y_k^* = c) \neq \frac{\exp(y_c^*)}{\sum_{k=1}^K \exp(y_k^*)}. \quad (5)$$

Thus when we interpret the heteroscedastic classification model of Kendall and Gal [19] as a latent variable model, which it implicitly is, we see that the computation of the predictive probabilities are not theoretically justified as it is unclear what the underlying data generation process is.

### 3 Softmax as a Smooth Approximation to the Data Generation Process

We have seen that the existing state-of-the-art deep heteroscedastic classification model is inexact when interpreted as a latent variable model. We argue that this model should be viewed as a special case of a smooth approximation to the assumed data generation process.

Computing  $p_c$  in Eq. (3) requires an integral over  $\epsilon_c$  which in general cannot be computed analytically [32]. This integral is an expectation over the unobserved component of utility, which can be estimated with Monte Carlo methods. However, MC estimation still has the additional issue that the arg max function's derivatives are either zero or undefined. Therefore we seek a smooth approximation to the arg max in Eq. (3). Similar to the development of the Gumbel-Softmax [17, 26], we note that in a zero temperature limit the softmax function is equivalent to the argmax, hence:

$$\begin{aligned} p_c &= P(\arg \max_k y_k^* = c) = \mathbb{E} \left[ \mathbb{1} \left\{ \arg \max_k y_k^* = c \right\} \right] \\ &= \mathbb{E} \left[ \lim_{\tau \rightarrow 0} \frac{\exp(y_c^*/\tau)}{\sum_{k=1}^K \exp(y_k^*/\tau)} \right] \approx \mathbb{E} \left[ \frac{\exp(y_c^*/\tau)}{\sum_{k=1}^K \exp(y_k^*/\tau)} \right], \quad \tau > 0. \end{aligned} \quad (6)$$

The expectation above is over  $\mathbb{E}_{\epsilon_1 \sim \mathcal{N}(0, \sigma_1^{\mathbf{w}}(\mathbf{x})), \dots, \epsilon_K \sim \mathcal{N}(0, \sigma_K^{\mathbf{w}}(\mathbf{x}))}$ .  $\mathbb{1}$  is a 0-1 indicator function. A similar result for binary classification with sigmoid smoothing function is derived in Appendix A. It is trivial to extend both derivations beyond the normal to all location-scale families of noise distribution. The softmax can be viewed as a smooth approximation to the true model, where the approximation is exact in a zero temperature limit and biased, but differentiable, for positive temperatures  $\tau$ .

**Estimating  $p_c$  and its gradient** We can rewrite  $y_c^*$  as a *deterministic* function  $g$ , of  $\mathcal{N}(0, 1)$ . We can thus apply the reparametrisation trick [20] allowing  $y_c^* = g(f_c^w(\mathbf{x}), \sigma_c^w(\mathbf{x}), u_c)$ ,  $u_c \sim \mathcal{N}(0, 1)$ , a MC estimate of the approximate predictive probabilities  $p_c$  can be obtained:

$$p_c \approx \frac{1}{S} \sum_{s=1}^S \frac{\exp(g(f_c^w(\mathbf{x}), \sigma_c^w(\mathbf{x}), u_c^s)/\tau)}{\sum_{k=1}^K \exp(g(f_k^w(\mathbf{x}), \sigma_k^w(\mathbf{x}), u_k^s)/\tau)}, \quad u_1^s, \dots, u_K^s \sim \mathcal{N}(0, 1). \quad (7)$$

Due to the reparametrization trick, the gradients for Eq. (7) w.r.t.  $w$  can be computed. Once we have computed  $f_c^w(\mathbf{x})$  and  $\sigma_c^w(\mathbf{x})$ , computing Eq. (7), with  $S$  samples, has computational complexity  $\mathcal{O}(SK)$ . This is typically trivial relative to the complexity of computing  $f_c^w(\mathbf{x})$  and  $\sigma_c^w(\mathbf{x})$ . For example if  $f_c^w$  and  $\sigma_c^w$  are neural networks with  $L$  fully-connected layers of dimension  $D$  (assuming input dimension is also  $D$ ) then the complexity of computing  $f_c^w(\mathbf{x})$  and  $\sigma_c^w(\mathbf{x})$  is  $\mathcal{O}(LD^2 + DK)$ , which for deep networks dwarfs  $\mathcal{O}(SK)$ . We can thus reduce the variance of Eq. (7), by taking many MC samples, with little impact on the training or inference time.

**Bias-variance trade-off** In our softmax approximation, as the temperature  $\tau$  gets closer to zero, the bias in the approximation to the true objective goes down, but the variance of the MC estimate of the gradients of the approximate objective increases [17, 26]. The temperature parameter essentially controls a bias-variance trade-off. It is important to emphasize that the model of Kendall and Gal [19], Eq. (2), can be viewed as a special case of this approximation with  $\tau = 1.0$ . However the authors do not motivate their model as an approximation to a true model or recognise the importance of the temperature parameter in controlling that approximation. Tuning this temperature may enable us to find a better point along this trade-off than always setting  $\tau = 1.0$ .

Similar approximations, with linear function approximators, have been studied in the the econometrics literature [5, 27, 32]. The latent variable formulations of heteroscedastic classification models is also standard in the Gaussian Process literature where naturally it is assumed the latent noise  $\epsilon_c$  is distributed Gaussian [15, 33] and a GP prior is placed on  $f(\mathbf{x})$  and  $\log \sigma(\mathbf{x})^2$ . Again exact inference on the likelihood is intractable and different approximate inference methods are used [15].

## 4 Related Work

### 4.1 Aleatoric Uncertainty in Deep Learning

Estimating uncertainty in deep learning has mostly focused on epistemic uncertainty [4, 11]. Nevertheless, for heteroscedastic regression Bishop and Quazaz [3] were early proponents of parameterizing the mean and variance term in a Gaussian likelihood with neural networks.

Follow-up work [19] revisits this regression model and introduces the heteroscedastic classification model discussed earlier in this paper. The authors show that these heteroscedastic models can be combined with MC dropout [11] approximate Bayesian inference for epistemic uncertainty estimation. The combined heteroscedastic Bayesian model yields improved performance on semantic segmentation and depth regression tasks. Lakshminarayanan et al. [22] propose an ensembling approach to uncertainty estimation in deep learning using multiple models to estimate both aleatoric and epistemic uncertainty. Along the same lines Liu et al. [25] introduce a Bayesian non-parametric ensemble to estimate both sources of uncertainty. Ayhan and Berens [1] propose estimating heteroscedastic aleatoric uncertainty by measuring the variation in the network’s output under standard data augmentation.

Finally, some recent research efforts aim to estimate specific uncertainty metrics. For example, Pearce et al. [29] introduce a novel loss function, which allows them to use ensemble networks to estimate prediction intervals without making any assumptions on the output distribution. Tagasovska and Lopez-Paz [31] introduce a quantile regression loss function in order to simultaneously learn all the conditional quantiles that are subsequently used to compute well-calibrated prediction intervals.

### 4.2 Noisy Labels

A large literature exists, which seeks to tackle the problem of classification with noisy labels using deep neural networks. Most of the methods try to identify samples with incorrect labels and remove or under-weight these samples in the loss function. Bootstrapping [30] attempts to denoise the labels by setting the target label to be a linear combination of the (potentially noisy) label and the current

model’s predictions. The MentorNet method [18] introduces a second neural network, the MentorNet, which estimates a curriculum learning strategy of weighting examples for training a StudentNet (i.e., the main network). The MentorNet can be learned to approximate a pre-defined curriculum or discover a new curriculum from data. In the latter case the curriculum is learned using a small dataset with clean labels. The Co-teaching method [14] also jointly trains two neural networks. At each training step, both networks compute predictions on a mini-batch of samples and identify small loss samples, which are then feed to the other network for learning. The underlying assumption is that small loss examples are more likely to have clean labels.

Note that our method can be applied to this problem of classification with noisy labels. However we highlight that our method also provides estimates of aleatoric uncertainty, which for some applications, may be an object of interest in its own right. Unlike some methods in the noisy labels literature, our method can be *naturally* combined with Bayesian methods for epistemic uncertainty estimation. We provide empirical comparisons with these methods in the next section.

## 5 Experiments

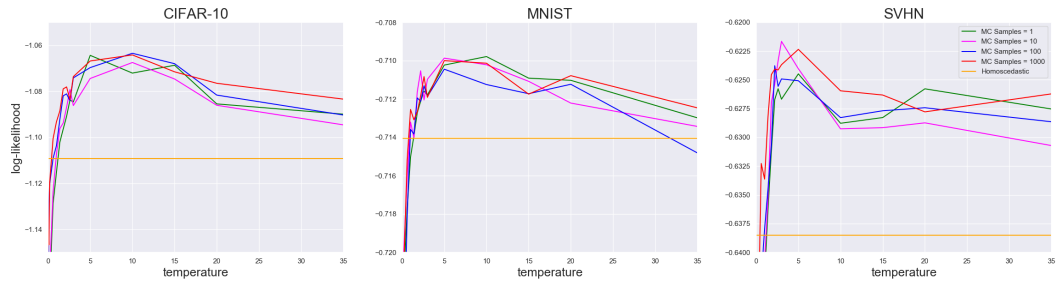


Figure 1: Effect of temperature and number of training MC samples on *noisy* test set log-likelihood.

In real-world applications of machine learning noisy labelled datasets are the norm, however public classification datasets are typically collected in such a manner as to avoid noisy labels. In the below experiments we evaluate our model on three image classification datasets (CIFAR-10, MNIST, SVHN) where we generate heteroscedasticity synthetically. We also evaluate our model on two image segmentation benchmarks which exhibit heteroscedasticity naturally [19], PASCAL VOC [9] and Cityscapes [8]. In general it is difficult to know *a priori* whether a real world dataset will exhibit heteroscedasticity. We address this question in Appendix B. We show that common problems with real world datasets such as noisy human labellers and missing not at random (*MNAR*) data satisfy the necessary conditions for heteroscedasticity.

### 5.1 Controlled Label Noise

We generate heteroscedasticity synthetically in three standard image classification datasets; CIFAR-10 [21], MNIST [23] and SVHN [28]. We corrupt the labels of some examples in a data-conditional manner as follows: examples with labels 0-4 are left uncorrupted, then for examples with labels 5-9 we randomly assign a new label with some probability. For examples with label 5, 20% of training examples were assigned a label from a uniform distribution over labels 0-9. 30%, 40%, 50% and 60% of labels 6, 7, 8 and 9 receiving the same treatment respectively. We use the same architecture as a baseline from the noisy labels literature [14], see Appendix D for details.

Fig. 1 shows the noisy test set log-likelihood as a function of the softmax temperature, averaged over 25 training runs. The number of MC samples during training is varied. However when making predictions on the test set and the validation set we always use 1,000 samples. The plots show a characteristic curve of a bias-variance trade-off, confirming the role and importance of the softmax temperature. Our method is also robust to the number of MC samples during training. See Appendix C for similar plots for test set accuracy. Table 1 shows the log-likelihood and accuracy on the noisy test set and accuracy on the clean test set for all methods including baselines from the noisy labels literature. In what follows, we further discuss the results shown in Fig. 1 and Table 1.

Table 1: Performance of each method on the CIFAR-10, MNIST and SVHN test datasets. Noisy log-likelihood (LL) and noisy accuracy (Acc) are computed on the noisy test set (with the same label corruption process applied to the training set). Clean accuracy ( $\text{Acc}_{\text{clean}}$ ) is computed on the test set with uncorrupted labels. For our method, optimal  $\tau^*$  is determined on the validation set. Number of samples  $S = 1000$ .  $p$ -values are from a paired sample two-tailed t-test with 25 replicates from corresponding random seeds. T-tests are conducted in reference to our method.

| Method               | CIFAR-10 ( $\tau^* = 5$ ) |                    |                             | MNIST ( $\tau^* = 10$ ) |                    |                             | SVHN ( $\tau^* = 5$ ) |                    |                             |
|----------------------|---------------------------|--------------------|-----------------------------|-------------------------|--------------------|-----------------------------|-----------------------|--------------------|-----------------------------|
|                      | LL                        | Acc                | $\text{Acc}_{\text{clean}}$ | LL                      | Acc                | $\text{Acc}_{\text{clean}}$ | LL                    | Acc                | $\text{Acc}_{\text{clean}}$ |
| Homoscedastic        | -1.109 <sup>‡</sup>       | 0.692 <sup>‡</sup> | 0.838 <sup>‡</sup>          | -0.714 <sup>‡</sup>     | 0.817*             | 0.993                       | -0.639 <sup>‡</sup>   | 0.836 <sup>‡</sup> | 0.951 <sup>‡</sup>          |
| $\tau = 1.0$ [19]    | -1.093 <sup>‡</sup>       | 0.695 <sup>†</sup> | 0.842 <sup>‡</sup>          | -0.713 <sup>‡</sup>     | <b>0.818</b>       | 0.993                       | -0.634 <sup>‡</sup>   | 0.837 <sup>‡</sup> | 0.952 <sup>†</sup>          |
| Ours $\tau = \tau^*$ | <b>-1.067</b>             | <b>0.702</b>       | <b>0.853</b>                | <b>-0.710</b>           | <b>0.818</b>       | <b>0.994</b>                | <b>-0.622</b>         | <b>0.839</b>       | <b>0.955</b>                |
| Co-teaching [14]     | -2.225 <sup>‡</sup>       | 0.696*             | 0.845 <sup>†</sup>          | -1.535 <sup>‡</sup>     | 0.817 <sup>†</sup> | 0.992 <sup>†</sup>          | -1.682 <sup>‡</sup>   | 0.835 <sup>‡</sup> | 0.950 <sup>†</sup>          |
| MentorNet [18]       | -2.116 <sup>‡</sup>       | 0.696 <sup>†</sup> | 0.843 <sup>‡</sup>          | -1.157 <sup>‡</sup>     | 0.817*             | 0.992 <sup>†</sup>          | -0.986 <sup>‡</sup>   | 0.836 <sup>†</sup> | 0.952*                      |
| Bootstrp. [30]       | -1.105 <sup>‡</sup>       | 0.697*             | 0.847*                      | -0.720 <sup>‡</sup>     | <b>0.818</b>       | <b>0.994</b>                | -0.637 <sup>‡</sup>   | 0.838              | <b>0.955</b>                |

\*  $p < 0.05$     †  $p < 0.01$     ‡  $p < 0.001$

### 5.1.1 Do Heteroscedastic Models Outperform Homoscedastic Models When There Exists Heteroscedastic Noise?

First we wish to verify whether in fact heteroscedastic models outperform the standard homoscedastic model when we know there exists heteroscedastic noisy labels. Looking at Fig. 1 it is clear that there are large ranges of temperatures for which the heteroscedastic test set log-likelihood is higher than the homoscedastic model. This is true for all numbers of training set MC samples. See Fig. 6 in Appendix C for similar plots for test set accuracy.

We also conduct a more formal test. We select the optimal temperature for each dataset based on the *validation set* log-likelihood. Then we conduct a paired sample t-test between the homoscedastic model and the heteroscedastic model at the optimal temperature on the *test set*, with  $S = 1000$ . Replicates in the t-test are paired by having corresponding random seeds. In Table 1 we see that for each dataset the best heteroscedastic model does in fact outperform the homoscedastic model and that the difference in test set log-likelihood and accuracy is statistically significant.

### 5.1.2 Is 1.0 Always the Optimal Temperature?

In addition to comparing our method to the homoscedastic baseline, we wish to compare to Kendall and Gal [19] who implicitly set the softmax temperature to 1.0. We again select the optimal temperature on the validation set and then perform a paired t-test between the heteroscedastic model at optimal temperature and at  $\tau = 1.0$  on the test set.

Table 1 shows that the optimal temperature is greater than 1.0 on all datasets and the difference in log-likelihood between the optimal temperature and  $\tau = 1.0$  is statistically significant on all datasets. Thus the optimal temperature is not always 1.0 and the performance of heteroscedastic models can be improved by tuning the softmax temperature, as claimed. Image segmentation results reported below also confirm this.

### 5.1.3 Heteroscedastic vs. Noisy Labels Baselines

In addition to comparing against a homoscedastic baseline and the previous best heteroscedastic method in the literature [19] we also compare against three baselines from the noisy labels literature; Co-teaching [14], Self-Paced MentorNet [18] and Bootstrapping [30]. These methods are reviewed in §4.2. Implementation details for each baseline are given in Appendix D. We note that unlike our method, these baselines do not give a principled measure of aleatoric uncertainty and are less naturally combined with Bayesian methods for epistemic uncertainty estimation, but are nonetheless empirically successful methods for handling noisy labels.

Our method compares favourably to each baseline when evaluated on the noisy test set. However, these baselines mainly target making predictions on a clean test set. Our method can be directly

applied to a clean test set, but will not give calibrated predictions unless the  $\sigma_c^w(x)$  terms are tuned on a clean dataset. We avoid requiring an auxiliary dataset and report only accuracy on the clean test set for this reason (this is standard in the noisy labels literature). Our method has higher clean test set accuracy than the other baselines, tying with Bootstrapping on two datasets. Both Co-teaching and MentorNet use different heuristics to estimate which examples have noisy labels and then prevent further training on these examples. One interpretation of our method is as a smooth version of this process, whereby the network can use its own predicted aleatoric uncertainty to down-weight an example in the loss function, smoothly including/excluding examples from further training. Under our input-dependent label noise generation process, our method outperforms the previous state-of-the-art method for heteroscedastic aleatoric uncertainty modelling for deep classifiers *and* the state-of-the-art methods for training deep classifiers with noisy labels.

**Additional results** We provide additional results with controlled label noise in appendices C.1, C.2 and C.3. Our model results in improved test set log-likelihood and accuracy on the original MNIST, CIFAR-10 and SVHN datasets, *even when no noise is added to the labels* (Appendix C.1). We also show the utility of our model when the controlled label noise is uniform/homoscedastic (Appendix C.2) and we validate that as the level of heteroscedastic noise in the labels is increased our model provides increasing improvements over the baselines (Appendix C.3).

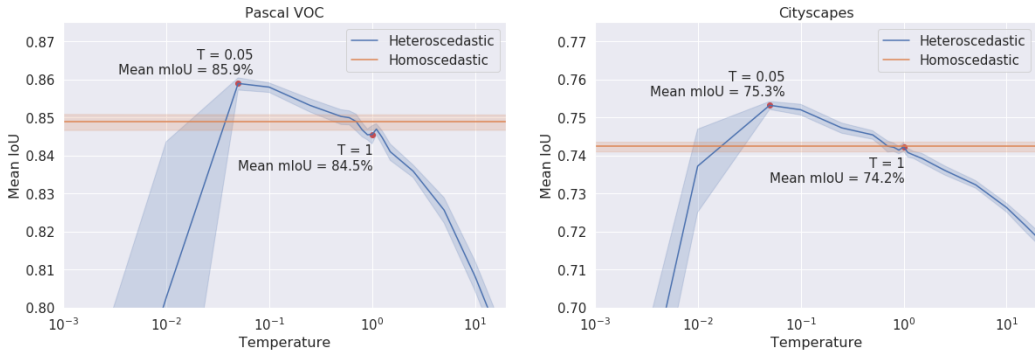


Figure 2: Validation set image segmentation mIoU on PASCAL VOC and Cityscapes datasets. Results are averaged over 25 random seeds. The shaded area shows bootstrapped 95% confidence intervals.

## 5.2 Image Segmentation

Table 2: Image segmentation results for heteroscedastic and homoscedastic models.  $p$ -values are from a paired sample two-tailed t-test where replicas are from corresponding random seeds. 25 replicates are used. T-tests are conducted w.r.t. the heteroscedastic mIoU at optimal  $\tau^*$ . The number of test server submissions is limited, so we only report  $p$ -values for the validation set.  $\ddagger p < 0.001$ .

| Dataset    | $\tau^*$ | Validation           |                 |              | Test                 |                 |              |
|------------|----------|----------------------|-----------------|--------------|----------------------|-----------------|--------------|
|            |          | $mIoU_{\tau=\tau^*}$ | $mIoU_{\tau=1}$ | $mIoU_{Hom}$ | $mIoU_{\tau=\tau^*}$ | $mIoU_{\tau=1}$ | $mIoU_{Hom}$ |
| Cityscapes | 0.05     | 75.32% $^{\ddagger}$ | 74.22%          | 74.24%       | 77.35%               | 76.36%          | 76.61%       |
| PASCAL VOC | 0.05     | 85.89% $^{\ddagger}$ | 84.55%          | 84.89%       | 84.65%               | 83.93%          | 84.01%       |

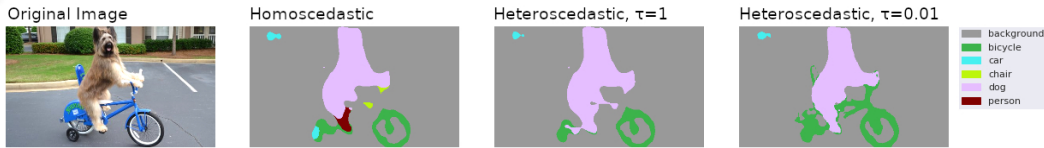


Figure 3: Image segmentation for an image from the internet (not in the PASCAL VOC dataset).

Image segmentation datasets have naturally occurring data-dependent/heteroscedastic uncertainty. It is too time-consuming for a human annotator to individually label pixels (requiring 262,144 labelling

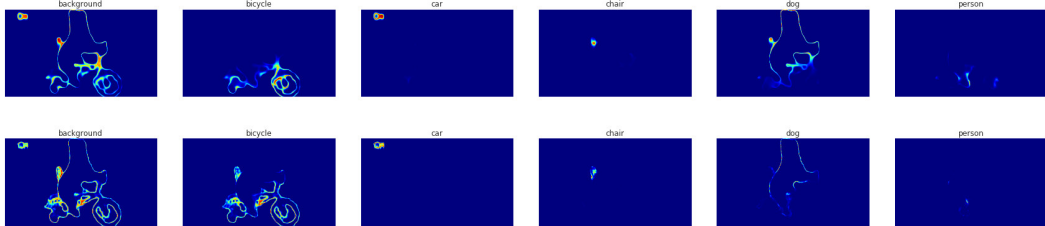


Figure 4: Heatmaps of aleatoric uncertainty (per class variance) for two heteroscedastic models corresponding to  $\tau = 1.0$  (top) and the optimal temperature  $\tau^* = 0.05$  (bottom).  $S = 1000$ .

operations for a single  $512 \times 512$  image). In practice human annotators label collections of pixels at a time. As a result annotations tend to be noisy at the boundaries of objects.

We apply our heteroscedastic model to PASCAL VOC 2012 [9] and Cityscapes [8], two popular image segmentation benchmarks. We follow the same end-to-end image segmentation architecture and experimental setup as in Chen et al. [6], with the only difference being the application of our heteroscedastic sampling process to the model output; see Appendix E.1 for details. Performance is measured by mean Intersection over Union (mIoU).

Figure 2 shows the effect of the softmax temperature on segmentation quality, using  $S = 1000$  MC samples for the heteroscedastic method. Again we observe a classic trade-off curve with an optimal temperature in-between two extremes of bias and variance. Heteroscedastic models outperform the homoscedastic model for a range of temperatures. Similar to the controlled label noise experiments, the optimal temperature  $\tau^*$  is not 1.0. Furthermore, for both datasets,  $\tau = 1.0$  is outperformed by the *homoscedastic* model on average. Table 2 shows that the differences in performances between the heteroscedastic model at the optimal temperature, the heteroscedastic model at  $\tau = 1.0$  and the homoscedastic model are statistically significant. We report both validation set and test set results as the number of submissions to the test server is limited, which does not enable us to test the importance of the temperature parameter or compute p-values.

The difference in the models also leads to qualitatively different segmentations and uncertainty heatmaps. Fig. 3 shows an example segmentation, using the best homoscedastic, heteroscedastic at  $\tau = 1.0$  and at  $\tau^* = 0.05$  models trained on PASCAL VOC. Reflecting the improvement in mean IoU the heteroscedastic segmentation at optimal temperature is qualitatively superior. Further examples are shown in Appendix E.2 where we have selected both success and failure cases.

Image segmentation provides a natural example of the additional advantages (other than improved predictive performance) of our method vs. other methods in the noisy labels literature. Our method also provides an estimate of aleatoric uncertainty. Fig. 4 demonstrates this, showing heat maps of per-class variance of the predictive distribution. As expected, the regions of highest aleatoric uncertainty are at object boundaries. Interestingly, the heteroscedastic uncertainty heatmaps at optimal temperature are more fine grained and precise than the  $\tau = 1.0$  heatmaps.

## 6 Conclusion

We have argued that the true generative model of latent variable heteroscedastic classification models involves an argmax over latent variables and that the softmax should be viewed as an approximation to this argmax. This approximation is equivalent in a zero temperature limit but in practice the temperature must be tuned to balance bias in the approximation and the variance of the gradients. The model of Kendall and Gal [19] can be viewed as a special case of our method with  $\tau = 1.0$ .

By interpreting the previous best deep heteroscedastic classification model as an approximation to a well understood generative process we place this model on firmer theoretical footing. Under our theory, we tune the softmax temperature to control a bias-variance trade-off, and by doing so, we have shown improved performance on a range of image classification tasks with controlled label noise. Our method also improves classification performance on these benchmark datasets when no noise is added to the labels. On two image segmentation datasets with naturally occurring heteroscedasticity, tuning the softmax temperature results in qualitatively and quantitatively improved segmentations.

## Broader Impact

This work proposes a novel probabilistic framework for modeling aleatoric uncertainty in classification tasks using deep neural networks. Our research could be applied to a wide range of applications including safety critical applications, such as self-driving cars, to more general ones, such as image classification, image segmentation as well as general classification tasks that may involve label noise.

**Benefits** Quantifying uncertainty can be particularly important in safety critical applications. For example, in self-driving cars when an object can not be confidently recognized, an alert could be raised asking for human intervention in order to avoid car accidents; hence saving lives. More broadly, when the model is not certain about its predictions, it may be better to abstain from making a decision, rather than making one with high uncertainty.

**Risks** On the other hand, if the system is used by someone who does not understand the notion of uncertainty to a sufficient level, then the system may be misused.

**Initiatives** We encourage further research in establishing rigorous evaluation protocols for uncertainty quantification. More broadly, we also encourage educational initiatives that will explain the limitations that current AI systems have.

## References

- [1] Murat Seckin Ayhan and Philipp Berens. Test-time Data Augmentation for Estimation of Heteroscedastic Aleatoric Uncertainty in Deep Neural Networks. *1st Conference on Medical Imaging with Deep Learning (MIDL)*, 2018.
- [2] Chandra R Bhat. A heteroscedastic extreme value model of intercity travel mode choice. *Transportation Research Part B: Methodological*, 29(6):471–483, 1995.
- [3] Christopher M Bishop and Cazhaow S Quazaz. Regression with input-dependent noise: A bayesian treatment. In *Advances in neural information processing systems*, pages 347–353, 1997.
- [4] Charles Blundell, Julien Cornebise, Koray Kavukcuoglu, and Daan Wierstra. Weight uncertainty in neural networks. In *Proceedings of the 32nd International Conference on Machine Learning-Volume 37*, pages 1613–1622, 2015.
- [5] Moshe Ben-Akiva and Denis Bolduc. Multinomial probit with a logit kernel and a general parametric specification of the covariaticce structure. Technical report, MIT Working Paper, 1996.
- [6] Liang-Chieh Chen, Yukun Zhu, George Papandreou, Florian Schroff, and Hartwig Adam. Encoder-decoder with atrous separable convolution for semantic image segmentation. In *The European Conference on Computer Vision (ECCV)*, pages 801–818, 2018.
- [7] François Chollet. Xception: Deep learning with depthwise separable convolutions. In *The IEEE Conference on Computer Vision and Pattern Recognition (CVPR)*, July 2017.
- [8] Marius Cordts, Mohamed Omran, Sebastian Ramos, Timo Rehfeld, Markus Enzweiler, Rodrigo Benenson, Uwe Franke, Stefan Roth, and Bernt Schiele. The cityscapes dataset for semantic urban scene understanding. In *The IEEE Conference on Computer Vision and Pattern Recognition (CVPR)*, June 2016.
- [9] Mark Everingham, S. M. Ali Eslami, Luc Van Gool, Christopher K. I. Williams, John Winn, and Andrew Zisserman. The pascal visual object classes challenge: A retrospective. In *International Journal of Computer Vision (IJCV)*, volume 111, pages 98–136, 2014.
- [10] Yarin Gal. *Uncertainty in deep learning*. PhD thesis, Department of Engineering, University of Cambridge, 2016.

- [11] Yarin Gal and Zoubin Ghahramani. Dropout as a bayesian approximation: Representing model uncertainty in deep learning. In *International Conference on Machine Learning*, pages 1050–1059, 2016.
- [12] Yarin Gal, Jiri Hron, and Alex Kendall. Concrete dropout. In *Advances in Neural Information Processing Systems*, pages 3581–3590, 2017.
- [13] William H Greene. *Econometric analysis, (Seventh ed.)*. Pearson Education Boston, 2012.
- [14] Bo Han, Quanming Yao, Xingrui Yu, Gang Niu, Miao Xu, Weihua Hu, Ivor W. Tsang, and Masashi Sugiyama. Co-teaching: Robust Training of Deep Neural Networks with Extremely Noisy Labels. *Advances in Neural Information Processing Systems (NIPS)*, 2018.
- [15] Daniel Hernández-Lobato, Viktoriia Sharmanska, Kristian Kersting, Christoph H Lampert, and Novi Quadrianto. Mind the nuisance: Gaussian process classification using privileged noise. In *Advances in Neural Information Processing Systems*, pages 837–845, 2014.
- [16] Sergey Ioffe and Christian Szegedy. Batch normalization: Accelerating deep network training by reducing internal covariate shift. In *International Conference on Machine Learning*, pages 448–456, 2015.
- [17] Eric Jang, Shixiang Gu, and Ben Poole. Categorical reparameterization with gumbel-softmax. In *Proceedings of the 5th International Conference on Learning Representations*, 2017. URL <https://arxiv.org/abs/1611.01144>.
- [18] Lu Jiang, Zhengyuan Zhou, Thomas Leung, Li-Jia Li, and Li Fei-Fei. MentorNet: Learning Data-Driven Curriculum for Very Deep Neural Networks on Corrupted Labels. *International Conference on Machine Learning (ICML)*, 2018.
- [19] Alex Kendall and Yarin Gal. What uncertainties do we need in bayesian deep learning for computer vision? In *Advances in Neural Information Processing Systems*, pages 5574–5584, 2017.
- [20] Diederik P Kingma, Max Welling, et al. Auto-encoding variational bayes. In *Proceedings of the International Conference on Learning Representations (ICLR)*, 2014.
- [21] Alex Krizhevsky. Learning multiple layers of features from tiny images. Technical report, University of Toronto, 2009.
- [22] Balaji Lakshminarayanan, Alexander Pritzel, and Charles Blundell. Simple and scalable predictive uncertainty estimation using deep ensembles. In *Proceedings of the 31st International Conference on Neural Information Processing Systems*, NIPS’17, page 6405–6416, Red Hook, NY, USA, 2017. Curran Associates Inc. ISBN 9781510860964.
- [23] Yann LeCun. The mnist database of handwritten digits. <http://yann. lecun. com/exdb/mnist/>, 1998.
- [24] Roderick JA Little and Donald B Rubin. *Statistical Analysis with Missing Data*, volume 333. John Wiley & Sons, 2014.
- [25] Jeremiah Liu, John Paisley, Marianthi-Anna Kioumourtzoglou, and Brent Coull. Accurate uncertainty estimation and decomposition in ensemble learning. In *Advances in Neural Information Processing Systems*, pages 8950–8961, 2019.
- [26] Chris J Maddison, Andriy Mnih, and Yee Whye Teh. The concrete distribution: A continuous relaxation of discrete random variables. In *Proceedings of the 5th International Conference on Learning Representations*, 2017. URL <https://arxiv.org/abs/1611.00712>.
- [27] Daniel McFadden. A method of simulated moments for estimation of discrete response models without numerical integration. *Econometrica: Journal of the Econometric Society*, pages 995–1026, 1989.
- [28] Yuval Netzer, Tao Wang, Adam Coates, Alessandro Bissacco, Bo Wu, and Andrew Y Ng. Reading digits in natural images with unsupervised feature learning. *Advances in Neural Information Processing Systems (NIPS)*, 2011.

- [29] Tim Pearce, Mohamed Zaki, Alexandra Brintrup, and Andy Neely. High-Quality Prediction Intervals for Deep Learning: A Distribution-Free, Ensembled Approach. *International Conference on Machine Learning (ICML)*, 2018.
- [30] S Reed, Honglak Lee, Dragomir Anguelov, Christian Szegedy, Dumitru Erhan, and Andrew Rabinovich. Training deep neural networks on noisy labels with bootstrapping. *arXiv preprint arXiv:1412.6596*, 2014.
- [31] Natasa Tagasovska and David Lopez-Paz. Single-model uncertainties for deep learning. *Advances in Neural Information Processing Systems (NeurIPS) 32*, 2019.
- [32] Kenneth E Train. *Discrete choice methods with simulation*. Cambridge university press, 2009.
- [33] Christopher KI Williams and Carl Edward Rasmussen. *Gaussian processes for machine learning*, volume 2. MIT press Cambridge, MA, 2006.
- [34] Yuxin Wu and Kaiming He. Group normalization. In *Proceedings of the European Conference on Computer Vision (ECCV)*, pages 3–19, 2018.

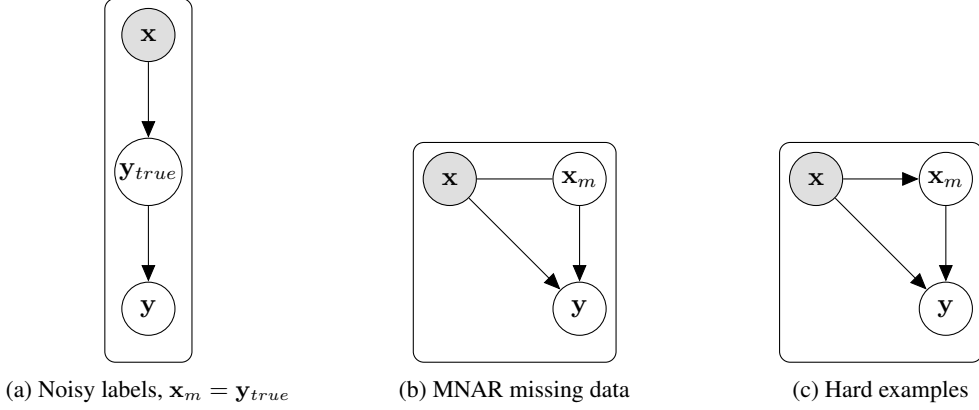


Figure 5: Example graphical models satisfying conditions for heteroscedasticity.

## A Heteroscedastic Binary Classification

For multi-class classification we use the softmax as a smoothing function for the argmax with the guarantee of equivalence in a zero temperature limit. For binary classification it is more convenient to avoid the use of the vector valued argmax and softmax functions and simply have the model output the probability of one class being chosen,  $p_1$ , in which case the probability of the other class is simply  $p_0 = 1 - p_1$ :

$$\begin{aligned}
 p_1 &= P(y_1^* > y_0^*) \\
 &= P(y_1^* - y_0^* > 0) \\
 &= P(y^* > 0) \\
 &= \mathbb{E}_{\epsilon \sim \mathcal{N}(0, \sigma_w(\mathbf{x}))} [\mathbb{1}\{y^* > 0\}] \\
 &= \mathbb{E}_{\epsilon \sim \mathcal{N}(0, \sigma_w(\mathbf{x}))} \left[ \lim_{\tau \rightarrow 0} \frac{1}{1 + \exp(-y^*/\tau)} \right] \\
 &\approx \mathbb{E}_{\epsilon \sim \mathcal{N}(0, \sigma_w(\mathbf{x}))} \left[ \frac{1}{1 + \exp(-y^*/\tau)} \right], \quad \tau > 0
 \end{aligned} \tag{8}$$

The key step is to replace the difference of the two latent variables  $y_1^* - y_0^*$  with a single latent variable  $y^*$  which is valid as all latent variables are members of the location-scale family  $\mathcal{N}$ . This sigmoid smoothing function has also been used in the econometrics literature [32].

## B Necessary Conditions for Heteroscedasticity

Given a classification task, it can be difficult to tell a priori whether the problem is heteroscedastic or homoscedastic. Here we state the necessary conditions for heteroscedasticity to exist. We also provide some graphical models that satisfy these conditions and correspond to reasonable models of real world applications. In practice it is always an empirical question as to whether some particular heteroscedastic model outperforms a homoscedastic model, but we hope these examples will provide a framework to think about heteroscedastic modelling and when it is likely to be helpful for a given task.

We wish to predict a label  $y$  given some observed variables  $\mathbf{x}$ . In order for us to be uncertain about the value of  $y$  there must be some other unobserved variables  $\mathbf{x}_m$  which influence  $y$ . If  $\mathbf{x}$  and  $\mathbf{x}_m$  are independent e.g. we assume  $\mathbf{x}_m$  is the source of additive  $Gumbel(0, 1)$  noise in a latent variable model then a heteroscedastic model won't help as we only observe  $\mathbf{x}$  which is independent of  $\mathbf{x}_m$ . Hence the necessary conditions for heteroscedasticity are  $\mathbf{x} \not\perp\!\!\!\perp y \wedge \mathbf{x}_m \not\perp\!\!\!\perp y \wedge \mathbf{x} \not\perp\!\!\!\perp \mathbf{x}_m$ .

Figure 5 shows some graphical models which satisfy these conditions. Our synthetically generated noisy labels are well modeled by Fig. 5a. Academic datasets typically do not have missing elements

in the input features. But when working on applications of machine learning, real world datasets very often having missing data. Interestingly datasets with missing not at random (MNAR) missingness [24] satisfy the necessary conditions for heteroscedasticity. Fig. 5b may be a reasonable graphical model for MNAR missing data where the missing components may be related in complex bi-directional relationships with the observed variables. Fig. 5c models cases such as image segmentation. Here the observed variables are predictive of imagined “true labels”, but we must deal with human labelled examples. In the image segmentation example, whether the pixel is at the boundary of an object (observed in  $x$ ) combined with unobserved features of the human labeller such as labelling method, speed of labelling, attention to detail, etc. interact to yield the observed labels.

## C Controlled Label Noise: Further Results

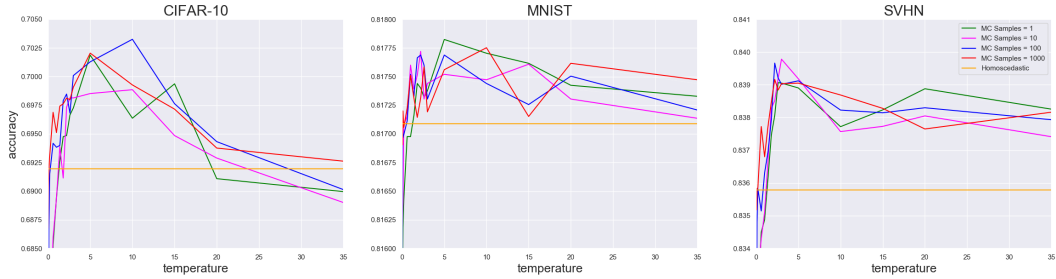


Figure 6: Effect of temperature and number of MC samples during training on *noisy* test set accuracy.

### C.1 No Noise

To test the generality of our method we evaluate it when trained on the original CIFAR-10, MNIST and SVHN datasets *without* corrupted labels, see Table 3 for results. Interestingly, we observe that our method leads to higher test set log-likelihood and accuracy compared to the homoscedastic and Kendall and Gal [19] baselines. This demonstrates that 1) our method can be applied to datasets with labels that are considered to be clean and still lead to performance improvements and 2) these datasets may have a source heteroscedasticity e.g. from ambiguous or hard to label examples.

Table 3: No noise. Performance of each method on the CIFAR-10, MNIST and SVHN clean test datasets. Log-likelihood (LL) and accuracy (Acc) are computed on the *clean* test set and all models are trained on the *clean* training set with no added label noise. For our heteroscedastic method, optimal  $\tau^*$  is determined on the validation set and  $S = 1000$ .  $p$ -values are from a paired sample two-tailed t-test with 25 replicates from corresponding random seeds. T-tests are conducted in reference to our method.

| Method               | CIFAR-10 ( $\tau^* = 5$ ) |              | MNIST ( $\tau^* = 3$ ) |              | SVHN ( $\tau^* = 5$ ) |                    |
|----------------------|---------------------------|--------------|------------------------|--------------|-----------------------|--------------------|
|                      | LL                        | Acc          | LL                     | Acc          | LL                    | Acc                |
| Homoscedastic        | -0.410 <sup>†</sup>       | 0.874        | -0.019                 | 0.994*       | -0.154 <sup>‡</sup>   | 0.961 <sup>†</sup> |
| $\tau = 1.0$ [19]    | -0.408*                   | 0.875        | -0.018                 | 0.994*       | -0.156 <sup>‡</sup>   | 0.960 <sup>†</sup> |
| Ours $\tau = \tau^*$ | <b>-0.390</b>             | <b>0.879</b> | <b>-0.017</b>          | <b>0.995</b> | <b>-0.143</b>         | <b>0.963</b>       |

\*  $p < 0.05$

†  $p < 0.01$

‡  $p < 0.001$

### C.2 Uniform Noise

We evaluate our method and all baselines on the image classification datasets under uniform/heteroscedastic noise, see Table 4. We randomly reassign 20% of labels to a label in 0-9 (with equal probability for each label). Our method performs competitively on this benchmark and outperforms the homoscedastic and  $\tau = 1.0$  baselines, as expected. However, the noisy labels baselines are stronger on this benchmark, in particular Co-teaching when evaluated on the noisy and clean accuracy. This demonstrates that different methods may perform better under different noise models. We

primarily target input dependent/heteroscedastic label noise. We note that in many applications the source of label noise is complex and likely input dependent and that simple scenarios such as uniform label noise may be unrealistic in practice.

Table 4: Uniform/homoscedastic noise. Performance of each method on the CIFAR-10, MNIST and SVHN test datasets corrupted with uniform noise. With 20% probability a label is flipped to a label from a uniform distribution over labels 0-9. Noisy log-likelihood (LL) and noisy accuracy (Acc) are computed on the noisy test set (with the same label corruption process applied to the training set). Clean accuracy ( $Acc_{clean}$ ) is computed on the test set with uncorrupted labels. For our method, optimal  $\tau^*$  is determined on the validation set. Number of samples  $S = 1000$ .  $p$ -values are from a paired sample two-tailed t-test with 25 replicates from corresponding random seeds. T-tests are conducted in reference to our method.

| Method               | CIFAR-10 ( $\tau^* = 35$ ) |                          |                    | MNIST ( $\tau^* = 35$ ) |                          |                    | SVHN ( $\tau^* = 5$ ) |                    |                    |
|----------------------|----------------------------|--------------------------|--------------------|-------------------------|--------------------------|--------------------|-----------------------|--------------------|--------------------|
|                      | LL                         | Acc                      | $Acc_{clean}$      | LL                      | Acc                      | $Acc_{clean}$      | LL                    | Acc                | $Acc_{clean}$      |
| Homoscedastic        | -1.232 <sup>‡</sup>        | 0.683 <sup>†</sup>       | 0.827 <sup>‡</sup> | -0.893 <sup>‡</sup>     | <b>0.814<sup>†</sup></b> | 0.993 <sup>*</sup> | -0.985 <sup>‡</sup>   | 0.780 <sup>‡</sup> | 0.950 <sup>‡</sup> |
| $\tau = 1.0$ [19]    | -1.204 <sup>†</sup>        | 0.689                    | 0.836 <sup>*</sup> | -0.891 <sup>‡</sup>     | <b>0.814<sup>*</sup></b> | 0.993 <sup>†</sup> | -0.974 <sup>‡</sup>   | 0.781 <sup>‡</sup> | 0.951 <sup>‡</sup> |
| Ours $\tau = \tau^*$ | <b>-1.186</b>              | 0.689                    | 0.842              | <b>-0.884</b>           | <b>0.814</b>             | <b>0.994</b>       | <b>-0.962</b>         | 0.784              | 0.955              |
| Co-teaching [14]     | -2.325 <sup>‡</sup>        | <b>0.700<sup>‡</sup></b> | <b>0.849</b>       | -1.730 <sup>‡</sup>     | 0.813 <sup>†</sup>       | 0.993 <sup>†</sup> | -1.974 <sup>‡</sup>   | <b>0.785</b>       | <b>0.956</b>       |
| MentorNet [18]       | -2.320 <sup>‡</sup>        | 0.696 <sup>*</sup>       | 0.846              | -1.202 <sup>‡</sup>     | <b>0.814</b>             | 0.993 <sup>*</sup> | -2.107 <sup>‡</sup>   | 0.784              | 0.955              |
| Bootstrp. [30]       | -1.236 <sup>‡</sup>        | 0.689                    | 0.836 <sup>*</sup> | -0.898 <sup>‡</sup>     | <b>0.814<sup>*</sup></b> | <b>0.994</b>       | -0.984 <sup>‡</sup>   | 0.782 <sup>†</sup> | 0.952 <sup>‡</sup> |

\*  $p < 0.05$     †  $p < 0.01$     ‡  $p < 0.001$

### C.3 Varying Noise Level

We vary the level of heteroscedastic noise to see the effect of using our model when there is a small/large amount of heteroscedastic noise relative to the results in the paper. Table 5 shows the results for a reduced level of heteroscedastic noise. In the main paper results are presented where labels 0-4 are left uncorrupted while labels 5-9 have 20%, 30%, 40%, 50% and 60% probability of being redrawn from a uniform distribution over all labels 0-9. For the results shown in Table 5, labels 0-4 are also left uncorrupted but the probability of corruption for the other labels is halved, so labels 5-9 have 10%, 15%, 20%, 25% and 30% probability of being redrawn from a uniform distribution over all labels 0-9. We see that with less heteroscedastic noise level, our method is still the best method or tied best method for all but the noisy accuracy metric on CIFAR-10, however the gap in performance between the methods is reduced.

Table 5: **Reduced** heteroscedastic noise. Performance of each method on the CIFAR-10, MNIST and SVHN test datasets corrupted with less heteroscedastic noise than in the main paper. Noisy log-likelihood (LL) and noisy accuracy (Acc) are computed on the noisy test set (with the same label corruption process applied to the training set). Clean accuracy ( $Acc_{clean}$ ) is computed on the test set with uncorrupted labels. For our method, optimal  $\tau^*$  is determined on the validation set. Number of samples  $S = 1000$ .  $p$ -values are from a paired sample two-tailed t-test with 25 replicates from corresponding random seeds. T-tests are conducted in reference to our method.

| Method               | CIFAR-10 ( $\tau^* = 20$ ) |              |                    | MNIST ( $\tau^* = 5$ ) |                          |                    | SVHN ( $\tau^* = 5$ ) |                    |                    |
|----------------------|----------------------------|--------------|--------------------|------------------------|--------------------------|--------------------|-----------------------|--------------------|--------------------|
|                      | LL                         | Acc          | $Acc_{clean}$      | LL                     | Acc                      | $Acc_{clean}$      | LL                    | Acc                | $Acc_{clean}$      |
| Homoscedastic        | -0.829 <sup>‡</sup>        | 0.783        | 0.860 <sup>*</sup> | -0.439 <sup>‡</sup>    | <b>0.907</b>             | 0.994              | -0.443 <sup>‡</sup>   | 0.898 <sup>‡</sup> | 0.956 <sup>‡</sup> |
| $\tau = 1.0$ [19]    | -0.811 <sup>†</sup>        | 0.786        | 0.864              | -0.438 <sup>†</sup>    | <b>0.907<sup>*</sup></b> | 0.994 <sup>*</sup> | -0.442 <sup>‡</sup>   | 0.898 <sup>‡</sup> | 0.957 <sup>‡</sup> |
| Ours $\tau = \tau^*$ | <b>-0.796</b>              | 0.785        | <b>0.865</b>       | <b>-0.434</b>          | <b>0.907</b>             | <b>0.995</b>       | <b>-0.430</b>         | <b>0.901</b>       | <b>0.960</b>       |
| Co-teaching [14]     | -1.329 <sup>‡</sup>        | <b>0.787</b> | <b>0.865</b>       | -0.791 <sup>‡</sup>    | 0.906 <sup>*</sup>       | 0.994 <sup>†</sup> | -0.905 <sup>‡</sup>   | 0.899 <sup>*</sup> | 0.959 <sup>*</sup> |
| MentorNet [18]       | -1.329 <sup>‡</sup>        | 0.781        | 0.864              | -0.574 <sup>‡</sup>    | 0.906 <sup>*</sup>       | 0.994 <sup>†</sup> | -0.883 <sup>‡</sup>   | 0.897 <sup>‡</sup> | 0.957 <sup>‡</sup> |
| Bootstrp. [30]       | -0.823 <sup>‡</sup>        | 0.786        | 0.863              | -0.441 <sup>‡</sup>    | <b>0.907</b>             | 0.994              | -0.441 <sup>‡</sup>   | 0.900              | 0.959              |

\*  $p < 0.05$     †  $p < 0.01$     ‡  $p < 0.001$

Table 6 shows the results for an increased level of heteroscedastic noise. For the results shown in Table 6, labels 0 and 1 are left uncorrupted and labels 2-9 have 5%, 15%, 25%, 35%, 45%, 55%, 65%, 75% probability of being redrawn from a uniform distribution over all labels 0-9. With this increased level of heteroscedastic noise, our method has best performance on all metrics for all datasets and the magnitude of the performance improvement from our method is increased relative to the reduced levels of heteroscedastic noise in the results in Table 5 and Table 1 in the main paper.

Table 6: **Increased** heteroscedastic noise. Performance of each method on the CIFAR-10, MNIST and SVHN test datasets corrupted with more heteroscedastic noise than in the main paper. Noisy log-likelihood (LL) and noisy accuracy (Acc) are computed on the noisy test set (with the same label corruption process applied to the training set). Clean accuracy (Acc<sub>clean</sub>) is computed on the test set with uncorrupted labels. For our method, optimal  $\tau^*$  is determined on the validation set. Number of samples  $S = 1000$ .  $p$ -values are from a paired sample two-tailed t-test with 25 replicates from corresponding random seeds. T-tests are conducted in reference to our method.

| Method               | CIFAR-10 ( $\tau^* = 10$ ) |                    |                      | MNIST ( $\tau^* = 5$ ) |                    |                      | SVHN ( $\tau^* = 5$ ) |                    |                      |
|----------------------|----------------------------|--------------------|----------------------|------------------------|--------------------|----------------------|-----------------------|--------------------|----------------------|
|                      | LL                         | Acc                | Acc <sub>clean</sub> | LL                     | Acc                | Acc <sub>clean</sub> | LL                    | Acc                | Acc <sub>clean</sub> |
| Homoscedastic        | -1.436 <sup>‡</sup>        | 0.583 <sup>‡</sup> | 0.796 <sup>‡</sup>   | -1.074 <sup>‡</sup>    | 0.713              | 0.990 <sup>†</sup>   | -0.980 <sup>‡</sup>   | 0.743 <sup>‡</sup> | 0.938 <sup>‡</sup>   |
| $\tau = 1.0$ [19]    | -1.417 <sup>‡</sup>        | 0.588 <sup>‡</sup> | 0.806 <sup>†</sup>   | -1.072 <sup>‡</sup>    | <b>0.714</b>       | 0.990 <sup>*</sup>   | -0.968 <sup>‡</sup>   | 0.744 <sup>‡</sup> | 0.940 <sup>‡</sup>   |
| Ours $\tau = \tau^*$ | <b>-1.383</b>              | <b>0.596</b>       | <b>0.818</b>         | <b>-1.067</b>          | <b>0.714</b>       | <b>0.991</b>         | <b>-0.956</b>         | <b>0.748</b>       | <b>0.946</b>         |
| Co-teaching [14]     | -3.399 <sup>‡</sup>        | 0.591 <sup>*</sup> | 0.810                | -2.310 <sup>‡</sup>    | 0.712 <sup>‡</sup> | 0.989 <sup>‡</sup>   | -2.630 <sup>‡</sup>   | 0.739 <sup>‡</sup> | 0.933 <sup>‡</sup>   |
| MentorNet [18]       | -3.115 <sup>‡</sup>        | 0.583 <sup>‡</sup> | 0.797 <sup>‡</sup>   | -1.156 <sup>‡</sup>    | 0.712 <sup>‡</sup> | 0.990 <sup>*</sup>   | -1.007 <sup>‡</sup>   | 0.732 <sup>‡</sup> | 0.944                |
| Bootstrp. [30]       | -1.454 <sup>‡</sup>        | 0.586 <sup>‡</sup> | 0.807 <sup>†</sup>   | -1.085 <sup>‡</sup>    | <b>0.714</b>       | <b>0.991</b>         | -0.981 <sup>‡</sup>   | 0.746 <sup>*</sup> | <b>0.946</b>         |

\*  $p < 0.05$     †  $p < 0.01$     ‡  $p < 0.001$

## D Controlled Label Noise Experiments: Architectural and Training Details

For all experiments on MNIST, CIFAR-10 and SVHN datasets we use a similar architecture to [14]. See Table 7 for details. We make one change, replacing the use of Batch Normalization [16] with Group Normalization [34] with 2 groups. The slopes of Leaky ReLU activation functions are set to 0.01.

We train with Adam with default parameters; learning rate = 0.001,  $\beta_1 = 0.9$ ,  $\beta_2 = 0.999$ ,  $\epsilon = 1e - 07$ . Networks are trained for a maximum of 1,000 epochs, being stopped early if validation set accuracy has not improved in 5 epochs. The best validation set checkpoint is used for test set evaluation.

Table 7: Covolutional network architectures used in experiments on MNIST, CIFAR-10 and SVHN datasets [14].

|   |
|---|
| $3 \times 3$ conv 128 filters, group norm, LReLU  |
| $3 \times 3$ conv 128 filters, group norm, LReLU  |
| $3 \times 3$ conv 128 filters, group norm, LReLU  |
| $2 \times 2$ max-pool, stride 2   |
| dropout, $p = 0.25$   |
| $3 \times 3$ conv 256 filters, group norm, LReLU  |
| $3 \times 3$ conv 256 filters, group norm, LReLU  |
| $3 \times 3$ conv 256 filters, group norm, LReLU  |
| $2 \times 2$ max-pool, stride 2   |
| dropout, $p = 0.25$   |
| $3 \times 3$ conv 512 filters, group norm, LReLU  |
| $3 \times 3$ conv 256 filters, group norm, LReLU  |
| $3 \times 3$ conv 128 filters, group norm, LReLU  |
| average-pool  |
| $f^w(x)$ : dense $128 \rightarrow 10$ , $\sigma^w(x)$ : dense $128 \rightarrow 10$ , softplus |

The MNIST dataset consists of 70,000 greyscale 28x28 images of handwritten numbers 0-9. We use the standard train/test split of 60,000 training images and 10,000 test set images. Of the 60,000 training images we use 10,000 as a validation set the remaining 50,000 are used for training. CIFAR-10 images are 32x32 colour images. We use the standard 10,000 CIFAR-10 test images, we use 10,000 of the 50,000 CIFAR-10 training examples as a validation set and the remaining 40,000 as the training set. SVHN images are also 32x32 colour images. We use the standard 26,032 test images and 10,000 of the images in the standard training set split as a validation set with the remaining 63,257 used as a training set. All images are scaled to  $[0, 1]$  by dividing elementwise by 255.

For heteroscedastic models we search over the following temperatures: 0.025, 0.05, 0.1, 0.2, 0.6, 1.0, 1.4, 1.8, 2.2, 2.6, 3.0, 5.0, 10.0, 15.0, 20.0, 35.0, 50.0, 100.0, picking the optimal temperature on the validation set.

For the Co-teaching baseline [14] we assume knowledge of the percentage of mis-labelled examples in the dataset and use this as the noise rate in the Co-teaching method. Similarly to the Co-teaching paper we allow  $T_k = 10$ , the number of epochs to linearly increase cutoff  $R(T)$ .

For the Bootstrap baseline [30], as per the original paper we set  $\beta = 0.8$ .

For the MentorNet baseline [18] we search over the following values for  $\lambda_2$ : 0.0, 0.5, 1.0, 2.0 and over 0, 5 and 10 epochs for the number of burn-in epochs. We set the decay factor to update the loss moving average to 0.9. We again assume knowledge of the percentage of mis-labelled examples in the dataset and use 1.0 - the noise rate as the quantile to determine the loss value to update the exponential moving average estimate of  $\lambda_1$ .

## E Image Segmentation

### E.1 Architecture and Training Details

We replicate the DeepLabv3+ [6] architecture and training setup which achieves state-of-the-art image segmentation results. DeepLabv3+ uses an Xception [7] based architecture with an added decoder module introduced. In particular we use the Xception65 architecture with an output stride of 16 [6]. The DeepLabv3+ method has three training stages; pretraining on JFT and MSCoco, followed by a training phase with output stride 16 (on augmented and/or coarsely labelled data) during which batch norm parameters are fine tuned. Finally, they train for 30K steps using the SGD optimizer with learning rate of 0.001 and otherwise default parameters. For experimentation, this final stage is trained at output stride 16, but models evaluated on the test server are trained with output stride 8 on the training and validation data. We warm start all our models from the end of the second training phase, and attempt to replicate the training set up discussed. We initially train on the train set and the fine-tune temperatures on the validation set; we then repeat this stage using the training & validation data using the best parameter settings from the validation set, and evaluate that on the test server.

In the homoscedastic model, a single convolution is applied to the output of a decoder, followed by bilinear upsampling to the size of the image, in order to compute logits for each pixel. For the heteroscedastic model, strictly speaking, either the final features should be upsampled to the original image size and used to compute correctly sized scale and location parameters, or the scale and location parameters should be computed at a lower dimension and upsampled to full size. However, this increases the number of MC samples required (by a factor of output stride), which makes it difficult to fit in the memory on a single device. We therefore sample the “logits” at a lower dimension and upsample to full image dimensions via bilinear interpolation.

## E.2 Image Segmentation Examples

